April 29, 1982

PHOENIX CORPORATION
1700 Old Meadow Road
McLean, Virginia 22102

FINAL REPORT
for
Contract No. NAS5-26579

GRAVSAT ERROR ANALYSIS
by means of
Global Spectral Analyses of the Marine Geoid
From Seasat Altimeter Data

Objective

This contract was to establish performance requirements for achieving a geoid accuracy of 10 cm with the GRAVSAT spacecraft. Specifically, this study will:

(1) Develop a data base using available Seasat-1 altimeter data from 400 repeat revolutions.

(2) Perform spectral analyses on all revs to assess the residual height energy at short wavelengths.

(3) Generate a global contour map of residual geoid power using results from spectral analysis.

Approach

A thorough spectral analysis of Seasat-I altimeter data on a global basis for suitable arc lengths serves to better delineate the geographic boundaries of regions with low residual geoid power at wavelengths too short to be represented in GRAVSAT measurements. By spectral analysis of Seasat altimeter data at frequent intervals along the 3 day repeating orbit arcs, it should be possible to define a dense grid of residual geoid power (geoid roughness) estimates for the world's oceans.

Summary of Work Performed

Seasat altimeter data provide a detailed and accurate measure of the instantaneous sea surface height every 3 km along the orbit track. These data comprise about 1500 orbit revolutions, most important of which are revolutions 1020 to 1501, the 3-day repeat orbit. In this orbit, a repeat track of altimeter data is generated every 3 days within a kilometer or two of previous tracks. Each colinear track measures essentially the same geoid, but different temporal ocean surface phenomena. The grid of 3-day repeat tracks has a spacing of 8.372 degrees of longitude. Brown, et al. [1981] have analyzed the variation of geoid roughness from these data in 5000 km arcs, finding a range

N83-15748
Unclas
CSCL 08E G3/43 00105
(E83-10105) GRAVSAT ERROR ANALYSIS BY MEANS OF GLOBAL SPECTRAL ANALYSES OF THE MARINE GEOID FROM SEASAT ALTIMETER DATA Final Report (Phoenix Corp.) 38 p HC A03/MF A01

of values from 170 cm RMS in the western Pacific to less than 7 cm RMS in the southeastern Pacific. However, these relatively long arcs prevent accurate delineation of local areas and lead to considerable anisotropy between ascending and descending passes over the same area.

However, if we break up these 3-day data arcs into 2 minute time intervals (800 km segments), then we can estimate the variability of the altimetric sea height power spectra at a resolution consistent with the orbit track spacing. Subsequent separation of the oceanic or temporal variation spectra from the geoid spectra would permit construction of a global map of the spatial variation of geoid roughness at the same resolution. The span of Seasat orbits from 1155 through 1369 was found to yield the best redundant coverage of the marine geoid. While the use of a 15 day span of data gives 5-fold redundancy in coverage of some areas, the presence of data gaps and otherwise unusable data in some of the arcs make the 15 day span a necessity. In fact, even with this long an arc, there are still some gaps in the North Atlantic coverage.

Before useful spectral analyses can be performed on these data, they must be reduced to sea surface heights relative to the reference ellipsoid. If long-wavelength orbit error is present in the altimetric geoid data, it can distort the shape and slope of the derived power spectrum, and cause erroneous estimation of the total short wavelength variance for that segment. Thus an accurate estimate of satellite altitude above the reference ellipsoid is required, a quantity which is usually not known to better than several meters. To overcome this difficulty, we have fit the sea surface heights derived from the altimeter data to a reference surface which approximates the shape of the geoid surface. This data processing is accomplished by fitting a low order function to the data, (see Brown [1982]) over a 6000 km pass comprising 8 short segments. Subsequent subtraction of this low order function from the data results in sea surface heights which are a least squares best fit to the GEM-10B geoid model (Lerch et al., 1978).

This orbit correction process is performed for 904 passes in the 15-day arc. Each of these passes has precisely defined start and stop points to ensure exact coincidence with passes from subsequent 3-day arcs. Passes which had suspiciously large residuals (>5 m RMS) relative to the GEM-10B geoid were deleted. There were no more than 17 such passes out of 904 processed in the 15 day arc. These were caused primarily by erroneous data on the altimeter tapes. Each 6000 km pass was then divided into exactly 8 segments at prescribed points for subsequent spectral analysis.

The altimetric geoid height data in each 2 minute segment was treated as a conventional time series for spectral analysis. Using a window which minimizes spectral leakage effects, a conventional periodogram analysis was used to construct the power

spectrum for wavelengths between 800 km and 7 km. The power represented here for a given frequency is the sum of squares of the coefficients of the sine and cosine terms of that frequency, and thus corresponds to a peak power. The average power, i.e. the mean square of the amplitudes over the segment, is just half the peak power. Note that the frequency is specified in cycles per revolution about the earth, which corresponds to the degree index of a spherical harmonic expansion. A power-law representation is then fitted to the spectrum between 50 and 1000 cycles per revolution, corresponding to the wavelength range 800 km to 40 km. This frequency range includes not only the geoid signal of interest, but the mesoscale temporal variations of the ocean and part of the white noise floor of the altimeter measurement as well. Note that the wavelengths of ocean tides are generally longer than 800 km, so they may be considered not to affect this spectral analysis.

Since the temporal phenomena and the noise tend to dominate the higher frequency range, we give higher weight to the lower frequencies in the power law fit. Such a weighting also tends to compensate for the over-representation of the higher frequencies in the periodogram analysis. A weight inversely proportional to frequency squared was adopted in fitting the power law. The slope of the power law agrees closely with the -3.04 slope predicted by Kaula's rule of thumb for a linear spectrum (Wagner, 1979).

The power-law for each short arc must be scaled-down by its proportion of a complete orbit to obtain a spectral energy estimate comparable with a global spectrum. We express this as the fraction of the segment length in seconds compared to the orbital period of 6045.2 seconds, and scale the power law accordingly (e.g. Wagner, 1979). The scaled power law is extrapolated and integrated for all wavelengths smaller than 220 km to obtain an estimate of the variance of geoid height in this short wavelength range. The square root of this quantity is termed the geoid roughness for that particular segment. This same analysis is performed for each of 5270 individual segments of the 15 day arc. Ignoring those segments which had data gaps greater than 6 seconds cumulative, 3011 roughness values were gridded (averaged) on a global map at 5 degree intervals, and contoured. The resulting geoid roughness map is shown in Figure 3 of the attached manuscript "Roughness of the Marine Geoid From Seasat Altimetry". Note that these roughness values are in terms of the square root of peak powers, and must be scaled by a factor of 0.707 to obtain roughness in terms of RMS of geoid heights.

The attached manuscript has been submitted for publication in the special Seasat issue of JGR. A paper of the same title was presented at the AGU meeting in San Francisco. It was well received, and seemed to be clearly understood by the audience. A letter was subsequently received from Professor Rapp which took issue with statements in our paper regarding treatment of GRAVSAT truncation errors. We responded to his letter, pointing out that

we had adopted a conservative approach to the estimate of aliasing due to truncation, whereas he had optimistically neglected it entirely. Professor Rapp acknowledged that the aliasing error due to truncation had been neglected, but would be treated in a forthcoming publication by Colombo. Our analysis in the geoid roughness paper had made the very conservative assumption that this error would be so large as to prevent recovery of any gravity features whose wavelength in smaller than about 200 km.

In preparation for future analyses (see Recommendations), the tapes of the SYNBAPS bathymetry data base were copied at GSFC. Associated documentation is being studied to transform meridional parts and Marsden squares to latitude and longitude for correlation analyses.

Conclusions

The variability of geoid power for wavelengths shorter than 220 km (geoid roughness), has been mapped for the world's oceans between latitudes 72°N and 72°S. A spectral analysis of Seasat altimeter data, reduced to sea surface heights, has been performed at 2 minute intervals for 15 consecutive days of the 3-day repeat orbit. The geoid roughness represented by these spectra for wavelengths shorter than about 220 km is separated from the total sea height variance and is displayed in the form of a global contour map. The global average geoid roughness is 32 cm RMS, varying from a high in excess of 2 m RMS near deep ocean trenches to a low of 2 cm RMS in the southeast Pacific near the East Pacific Rise. This average value agrees well with previous estimates based on gravimetry and GEOS-3 altimetry. In general, the smoothest areas in the marine geoid overlie relatively young seafloor adjacent mid-ocean spreading centers, where even short-wavelength topographic variations tend to be isostatically compensated.

The geoid roughness map can also be interpreted in terms of the error of omission in a satellite gravity (GRAVSAT) mission. In certain rather large areas of the southeast Pacific, the error of omission should be smaller than that over trenches and aseismic ridges. Insofar as the absolute roughness values can be trusted, we feel that the 10 cm geoid accuracy goal of the GRAVSAT mission can be satisfied best in the southeast Pacific.

Recommendations

There are additional analyses which can be performed on these data which are even more interesting for understanding the inner workings of the earth. Given the availability of detailed bathymetry from which depths along the satellite track can be inferred, it is feasible to calculate the cross-spectrum between the altimetric sea height and the bathymetry, and evaluate the

depth of compensation at various points along the data track. This could give rise to a related map showing the spatial variability of the depth of isostatic compensation, which has implications for the global patterns of crustal thickness and heat flow.

It is also possible to learn something more from the data processing already completed. I refer to the parameters of the power-law fit to the sea surface height covariance spectra. In particular, the exponent of the fit, which varies from -2.07 near the East-Pacific rise to <-5.0 in the Indian ocean geoid low, can be related to the depth of the underlying density structure. This is essentially due to the more rapid attenuation of short wavelength geopotential anomalies with depth. For example, a white noise distribution of density anomalies at the earth's surface that would exhibit a flat spectrum of geoid heights (zero slope), shows a spectrum of increasingly steeper slope as the density distribution is positioned at larger depths.

Some depth analyses have been performed using spectra of relatively long wavelength spherical harmonic geopotential models. Cook [1963] has shown from analysis of degree variance spectra of the low order geopotential that only anomalies of wavelength greater than 4000 km can originate as deep as the core-mantle interface. A higher degree model (SAO II) was analyzed by Allan [1972], who concluded that anomalies of wavelength greater than 7000 km are due to density fluctuations in the lower mantle, while anomalies of wavelength shorter than 7000 km can be generated by fluctuations in the asthenosphere. The nature of these spherical harmonic geopotential models is such that it is only possible to deduce density structure at asthenospheric depths and deeper, and then only in a global average sense.

In the field of aeromagnetic data interpretation, however, a different situation prevails. The existence of highly detailed aeromagnetic profiles and maps permits spectral analyses at shorter wavelengths, and the resolution of shallower depths for definite areas. At the same time, the existence of distinct and shallow horizons such as the Curie point and the boundary between crystalline and sedimentary rocks, result in relatively shallow depths of origin for magnetic anomalies. By postulating a statistical model of magnetic blocks of varying depth, width, thickness, and magnetization, it can be shown that the logarithm of the magnetic field energy spectrum is proportional to the depth of the ensemble of blocks. This technique has been widely used for determination of depth to magnetic basement. In principal, this method is equally applicable to analysis of geoid height profiles.

While density anomalies are not limited to such shallow depths, and they do not have such distinct horizons as magnetic anomalies, it should be possible to learn something about the variation of density structure within the crust simply by

analysis of the already existing set of spectral slope values. As with any new technique, some experimenting must be done to determine the proper interpretation of the derived depths. However, at the very least a global map of relative depth to density structure can be constructed which can have great value for interpretation of the tectonic provinces of the earth. In brief, we seem to have discovered a very fertile area for geophysical research: one which promises to bear fruit very quickly in terms of global marine maps of compensation depths and depths of density structure.

References

Allan, R.R., "Depth of Sources of Gravity Anomalies", Nature-Physical Science, 236, March 13, 1972.

Brown, R.D., W.D. Kahn, and W.E. Himwich, Variability of geoid and ocean surface spectra From Seasat-1 altimeter data EOS, 62(8), Feb. 24, 1981, p 80.

Brown, R.D., Ocean tides at Cobb seamount from Seasat altimetry, J. Geophys. Res., ( ), in press, 1982.

Cook, A.H., "Sources of Harmonics of Low Order in the External Gravity Field of the Earth", Nature, 198(4886), 1186, June 22, 1963.

Lerch, F.J., C.A. Wagner, S.M. Klosko, R.P. Belott, R.E. Laubscher, and W.A. Taylor, Gravity model improvement using GEOS-3 altimetry (GEM-10A and GEM-10B), paper presented at the 1978 Spring AGU Meeting, Miami, Florida, EOS, Trans. Am. Geophys. Union, 59(4), p260, 1978.

Wagner, C.A., The geoid spectrum from altimetry, J. Geophys. Res., 84, pp. 3864-3865, 1979.

ROUGHNESS OF THE MARINE GEOID FROM SEASAT ALTIMETRY

R. D. Brown, W. D. Kahn*, D. C. McAdoo*, and W. E. Himwich

Phoenix Corporation
1700 Old Meadow Road
McLean, Virginia 22102

Abstract

The geographical variability of short wavelength geoid power spectra (geoid roughness), has been mapped for the world's oceans between latitudes 72°N and 72°S. A spectral analysis of Seasat altimeter data, reduced to sea surface heights, has been performed at 2 minute intervals for 15 consecutive days of the 3-day repeat orbit. The geoid roughness represented by these spectra for wavelengths shorter than about 220 km is separated from the total sea height variance and is displayed in the form of a global contour map. The global average geoid roughness is 32 cm RMS, varying from a high in excess of 2 m RMS near deep ocean trenches to a low of 2 cm RMS in the southeast Pacific near the East Pacific Rise. This average value agrees well with previous estimates based on gravimetry and GEOS-3 altimetry. In general, the smoothest areas in the marine geoid overlie relatively young seafloor adjacent mid-ocean spreading centers, where even short-wavelength topographic variations tend to be isostatically compensated.

This study was sponsored by NASA Goddard Space Flight Center Geodynamics Branch under contract NAS5-26579.

* NASA Goddard Space Flight Center, Greenbelt, Md.

INTRODUCTION

The advent of satellite altimetry has provided an opportunity to map the marine geoid at scales as small as a few tens of kilometers with sub-decimeter precision. Since the fine structure of the geoid surface is sensitive to the depth of compensation of bathymetric features, we can begin to infer variations in depth of compensation and general structure of oceanic crust from satellite altimetry. Spectral analysis provides a convenient tool for evaluating these relationships, since it enables some separation of the geoid signal spectra from that of the altimeter noise and oceanographic effects. Wagner and Colombo [1979] have shown that it is possible to obtain accurate local estimates of the geopotential power spectrum from spectral analysis of GEOS-3 altimeter data. Here we apply spectral analysis to short arcs of Seasat altimeter to derive a preliminary map of the variability of the cumulative geoid power for scales less than 220 km (geoid roughness). Seasat altimeter data are much more precise than GEOS-3 data, permitting a more accurate separation of the short wavelength geoid signal from the altimeter noise and oceanographic effects. The following sections detail the procedure by which Seasat altimeter data are processed to construct the geoid roughness map. This map, derived from 15 consecutive days of Seasat data, is interpreted for error of omission of satellite gravity (GRAVSAT) missions as well as for depth of isostatic compensation of the ocean crust.

ALTIMETER DATA PROCESSING

Seasat altimeter data provide a detailed and accurate measure of the instantaneous sea surface height every 3 km along the orbit track. These data comprise about 1500 orbit revolutions, most important of which are revolutions 1020 to 1501, the 3-day repeat orbit (see Figure 1). In this orbit, a repeat track of altimeter data is generated every 3 days within a kilometer or two of previous tracks. Each colinear track measures essentially the same geoid, but different temporal ocean surface phenomena. The grid of 3-day repeat tracks has a spacing of 8.372 degrees of longitude. Brown, et al. [1981] have analyzed the variation of geoid roughness from these data in 5000 km arcs, finding a range of values from 170 cm RMS in the western Pacific to less than 7 cm RMS in the southeastern Pacific. However, these relatively long arcs prevent accurate delineation of local areas and lead to considerable anisotropy between ascending and descending passes over the same area.

However, if we break up these 3-day data arcs into 2 minute time intervals (800 km segments), then we can estimate the variability of the altimetric sea height power spectra at a resolution consistent with the orbit track spacing. Subsequent separation of the oceanic or temporal variation spectra from the geoid spectra would permit construction of a global map of the spatial variation of geoid roughness at the same resolution. The span of Seasat orbits from 1155 through 1369 was found to yield

the best redundant coverage of the marine geoid. The coverage from this span is shown in Figure 1, which also indicates the size of the 800 km segments. While the use of a 15 day span of data gives 3-fold redundancy in coverage of some areas, the presence of data gaps and otherwise unusable data in some of the arcs make the 15 day span a necessity. In fact, even with this long an arc, there are still some gaps in the North Atlantic coverage.

Orbit Error Correction

Before useful spectral analyses can be performed on these data, they must be reduced to sea surface heights relative to the reference ellipsoid. If long-wavelength orbit error is present in the altimetric geoid data, it can distort the shape and slope of the derived power spectrum, and cause erroneous estimation of the total short wavelength variance for that segment. Thus an accurate estimate of satellite altitude above the reference ellipsoid is required, a quantity which is usually not known to better than several meters. To overcome this difficulty, we have fit the sea surface heights derived from the altimeter data to a reference surface which approximates the shape of the geoid surface. This data processing is accomplished by fitting a low order function to the data, (see Brown [1982]) over a 6000 km pass comprising 8 short segments. Figure 1 shows an example of two such passes in the Pacific, their start and stop points denoted by the arrowheads on the orbit subtrack. Subsequent

subtraction of this low order function from the data results in sea surface heights which are a least squares best fit to the GEM-10B geoid model (Lerch et al., 1978).

This orbit correction process is performed for 904 passes in the 15-day arc. Each of these passes has precisely defined start and stop points to ensure exact coincidence with passes from subsequent 3-day arcs. Passes which had suspiciously large residuals (>5 m RMS) relative to the GEM-10B geoid were deleted. There were no more than 17 such passes out of 904 processed in the 15 day arc. These were caused primarily by erroneous data on the altimeter tapes. Each 6000 km pass was then divided into exactly 8 segments at prescribed points for subsequent spectral analysis.

Spectral Analysis

The altimetric geoid height data in each 2 minute segment was treated as a conventional time series for spectral analysis. Using a window which minimizes spectral leakage effects, a conventional periodogram analysis was used to construct the power spectrum for wavelengths between 800 km and 7 km. The spectrum for a typical segment is shown in Figure 2. The power represented here for a given frequency is the sum of squares of the coefficients of the sine and cosine terms of that frequency, and thus corresponds to a peak power. The average power, i.e. the mean square of the amplitudes over the segment, is just half

the peak power. Note that the frequency is specified in cycles per revolution about the earth, which corresponds to the degree index of a spherical harmonic expansion. A power-law representation is then fitted to the spectrum between 50 and 1000 cycles per revolution, corresponding to the wavelength range 800 km to 40 km. This frequency range includes not only the geoid signal of interest, but the mesoscale temporal variations of the ocean and part of the white noise floor of the altimeter measurement as well. Note that the wavelengths of ocean tides are generally longer than 800 km, so they may be considered not to affect this spectral analysis.

Since the temporal phenomena and the noise tend to dominate the higher frequency range, we give higher weight to the lower frequencies in the power law fit. Such a weighting also tends to compensate for the over-representation of the higher frequencies in the periodogram analysis. A weight inversely proportional to frequency squared was adopted in fitting the power law. The resulting power law, and its parameters for a typical segment in the South Atlantic, are shown in Figure 2. The slope of the power law agrees closely with the -3.04 slope predicted by Kaula's rule of thumb for a linear spectrum (Wagner, 1979).

Geoid Roughness Calculation

The power-law for each short arc must be scaled-down by its proportion of a complete orbit to obtain a spectral energy estimate comparable with a global spectrum. We express this as the fraction of the segment length in seconds compared to the orbital period of 6045.2 seconds, and scale the power law accordingly (e.g. Wagner, 1979). The scaled power law is extrapolated and integrated for all wavelengths smaller than 220 km to obtain an estimate of the variance of geoid height in this short wavelength range. The square root of this quantity is termed the geoid roughness for that particular segment. This same analysis is performed for each of 5270 individual segments of the 15 day arc. Ignoring those segments which had data gaps greater than 6 seconds cumulative, 3011 roughness values were gridded (averaged) on a global map at 5 degree intervals, and contoured. The resulting geoid roughness map is shown in Figure 3. Note that these roughness values are in terms of the square root of peak powers, and must be scaled by a factor of 0.707 to obtain roughness in terms of RMS of geoid heights.

There are several assumptions involved in the derivation of the geoid roughness which deserve examination. The first is that the proper description of the geoid spectrum is a power law. While this has not been verified, a power law was adopted because it is of the same form as Kaula's rule for the long wavelengths and is easily integrable. Until we can perform a more complete

separation of the spectra of the ocean surface variations from the geoid spectra, the adoption of a simple power law seems an adequate choice.

The second assumption is that the inverse frequency squared weighting fairly attenuates the mesoscale ocean surface variation spectra (50 to 500 km wavelength) and the altimeter noise spectra while allowing an accurate representation of the short wavelength geoid spectra. This is probably over-simplistic, but it is easy to implement, and it gives power law parameters which agree well, on average, with longer wavelength spectra. Given the precision of the power spectrum, it is an appropriate rule for a preliminary mapping of geoid roughness.

Finally, we must consider the uncertainty of the spectral analysis technique itself. It is well known that the use of any spectral analysis technique requires certain assumptions, e.g. periodicity of the data in the time series. Each technique also has its own set of heuristic rules which must be applied to obtain reasonable results. For example, the Blackman and Tukey [1958] method requires pre-whitening and smoothing windows. Least-squares spectral analysis, periodograms, fast Fourier transforms, etc. have similar special assumptions. If all these techniques were applied to the same data segment, the variation in results would probably exceed any error due to the above assumptions. The most important factor in conducting an investigation using spectral analyses is consistancy and

simplicity. Insofar as data are processed uniformly and minimally, results should be valid relatively, if not absolutely. Therefore, while the absolute values of the geoid roughness generated by this process may be in error, their relation to their neighbors (geographic variation) remains valid.

RESULTS

The geoid roughness map of Figure 3 is the spatial average of the roughness values of ascending and descending segments, redundant in general by a factor of 5. This map is displayed on a Van der Grinten projection for comparison with the physiography of National Geographic Society maps. The geoid roughness values are color coded (in cm) according to the key in the upper right corner of Figure 3.

The largest contrast in this map occurs between the geoid roughness of smooth regions like the southeast Pacific and rough areas like trenches. It is interesting to examine in greater detail the spectra of arc segments in these two regions. Figure 4 shows the spectra of a typical trench segment, superposed on spectra of a segment over the smooth flank of the East Pacific rise. The essential difference in these spectra is their slope, with trench regions exhibiting larger slopes (in an algebraic sense) than the global average. Figures 5a and 5b show the residual altimetric sea heights for the selected trench segment and the segment near the East Pacific rise.

The power law fit and integration shown in Figure 2 has been performed for each of 3011 arc segments. The global average slope of these power laws is -3.409, and the global average roughness is 45 cm (32 cm RMS), yeilding a global average power law given by

$$P = 132195\ f^{-3.409} \quad (m^2\ [\text{cycles per rev}]^{-1}) \qquad (1)$$

This power law, properly scaled for comparison with short arc spectra, is also plotted in Figure 4. The integrated power for wavelengths shorter than 220 km has been computed for each of these segments. This geoid variance has been assigned to the mid-point of the short arc segment and gridded in a 5 degree by 5 degree latitude-longitude grid. Thus 5 degree average variances are formed from the geoid variances of both ascending and descending arc segments, with up to five-fold redundancy in some areas. The variation of roughness between colinear segments is about 3 cm. Except near long linear features such as the Tonga-Kermadec trench, the variation between ascending and descending segments is remarkably small. The most severe anisotropy, 150 cm vs. 40 cm, occurs for this trench which parallels the descending arc segment. In other less lineated areas, the anisotropy is less than 10 cm.

INTERPRETATION

The short wavelength geoid roughness estimated in this study must of necessity be due to near-surface density variations of short wavelength in the crust and lithosphere. For example, we cite the spatial correlation between the distribution of geoid roughness mapped in Figure 3 and the degree of roughness of seafloor topography inferred from a global bathymetric chart. Deep ocean trenches represent sites of substantial short wavelength bathymetric relief and appear as highs on the geoid roughness map, Figure 3. This correlation is expected in view of the correlation generally found (McKenzie and Bowin [1976]) between bathymetry and shipborne gravimetric observations, and between bathymetry and altimetric geoid observations (e.g. Leitao and McGoogan [1974], Wagner [1979], Chapman and Talwani [1979]).

This geoid roughness map, however, contains more than just a confirmation of the gravity/bathymetry correlation. Regional variations in the depth of isostatic compensation can also be inferred

from the map. Over regions where isostatic compensation occurs only at substantial depth, if at all, high bathymetric relief equates to large values of short wavelength geoid variance. Conversely over regions where compensation depths are relatively shallow, high bathymetric relief does not result in large values of geoid roughness. For example, the East Pacific rise crest, while relatively rough in terms of bathymetric relief, is one of the smoothest areas of the geoid, due in part to its shallow isostatic compensation. This qualitative observation is quantified in the following paragraphs.

Isostatic Compensation Effects

In order to estimate the effect of compensation depth on the geoid power spectrum, let us assume that bathymetry varies in one dimension only and has a power spectrum equivalent to that of band-limited white noise (cf. Blackman and Tukey [1958] p79). The power spectrum is given by

$$P_b(f) = \frac{\sigma^2}{\pi f_c}\left(1 + \left[f/f_c\right]^2\right)^{-1} \qquad (2)$$

where f is frequency in cycles per unit length, σ^2 is the variance, and f_c is a cut-off frequency. Insofar as the bathymetric signal is to be passed through a linear system relating topography to the geoid, and the measured geoid has an effective cut-off frequency which is much lower than f_c, the bathymetric power spectrum may be approximated by

$$P_b(f) = \frac{\sigma^2}{\pi f_c} \tag{3}$$

In order to obtain the output geoid signal, the input bathymetric signal must be passed through a linear system (or filter) which is represented by a frequency response (or transfer) function, Y(f). Then the power spectrum, $P_g(f)$ of the geoid signal is given by

$$P_g(f) = |Y(f)|^2 P_b(f) \tag{4}$$

The transfer function, Y(f), in the case of uncompensated topography may be written as

$$Y_u(f) = C\exp(-2\pi|f|d)[|f|]^{-1} \tag{5}$$

where d is ocean depth and C is a constant described below. This function is obtained by multiplying the function defined in equation (12) of McKenzie and Bowin [1976], by the transfer function

$$S(f) = [2\pi g|f|]^{-1} \tag{6}$$

between gravity and the geoid (see Chapman [1979]). To represent the case of isostatic compensation, the transfer function

$$Y_c(f) = C\exp(-2\pi|f|d)\frac{(1 - \exp(-2\pi|f|T))}{|f|} \qquad (7)$$

is used, where T is the compensation depth below seafloor and

$$C = \Delta\rho G/g \qquad (8)$$

where $\Delta\rho$ is crustal density minus water density. The model in equation 7 is equivalent to that of simplified Airy compensation given by equation 13 of McKenzie and Bowin [1976] or equation 3 of Chapman and Talwani [1979]. The total geoid energy (or roughness) residing at frequencies above $|f| = f_o$ is

$$\mathcal{E} = 2\int_{f_o}^{\infty} P_g(f)df \qquad (9)$$

where $P_g(f)$ is given by equation 4 after substitutions from equations 3 and 5 or 7 as appropriate. The form of the integral in equation 9 is the exponential integral $E_2(z)$ defined and evaluated in Abramowitz and Stegun [1970], where $z=4\pi f_o d$ in the uncompensated case.

The square root of the short wavelength geoid roughness for various depths of compensation, T, is shown in Figure 6. This power function has been normalized by the residual geoid roughness from the uncompensated case. Values of d=5 km and f_o=0.0045 cycles/km have been adopted. The square root is displayed to allow a direct comparison with the geoid roughness map of Figure 3. This model suggests that short wavelength geoid

roughness will be substantially reduced if compensation depths are 30 km or less. On the other hand, if compensation occurs deeper than 40 km, the geoid roughness will essentially be that of the uncompensated case. Insofar as actual bathymetric power spectra are not white, but are stronger at long wavelengths (which are more likely to be compensated), the model estimates of the reduction of geoid roughness by compensation are conservative (smaller than reality).

Deep Ocean Trenches

Trenches are generally thought to be relatively uncompensated features (Vening-Meinesz [1964]). Certainly their effective depth of compensation is relatively large, if not infinite. From Figure 6 we see that the geoid roughness in this case is not appreciably reduced by isostasy. Furthermore, trenches generally constitute exceptionally high bathymetric relief. In this case it is not surprising that the major maxima in the geoid roughness map occur over large ocean trenches. In fact, the global maximum of geoid roughness (more than 200 cm) occurs over the Challenger Deep segment of the southern Marianas trench, which is the deepest point in the oceans. In general, a semi-quantitative relation is observed between the maximum depth of a given trench and its geoid roughness.

Mid-ocean Ridges

Another feature of the geoid roughness map is the broad region of low roughness (<20 cm) associated with mid-ocean ridges. Consider, for example, the East Pacific Rise and its ridge flanks. Cochran [1979] analyzed gravity and bathymetry in this region and found that isostatic compensation occurs at quite shallow depths, even shallower than those he estimated for the Mid-Atlantic ridge. In the case of the simplified Airy model, Cochran shows that a compensation depth of 10-20 km best fits the data for the East Pacific. According to model results in Figure 6, isostatic compensation at depths of 10-20 km should effectively halve the residual geoid roughness, compared to that of similar uncompensated bathymetric relief.

The region encompassing the Mid-Atlantic ridge and its flanks shows moderate values of geoid roughness (10-50 cm in the north and 10-30 cm in the south). The seafloor topography does not seem to be substantially rougher than that of the East Pacific Rise, but Cochran [1979] finds simplified Airy compensation depths of 20 to 50 km. Thus it appears that the disparity between geoid roughness over the Mid-Atlantic ridge and the East Pacific Rise is due in part to different depths of compensation. Cochran's analysis does not distiguish between the northern and the southern Mid-Atlantic ridge but in view of the smoother geoid in the south it is interesting to note that the

southern ridge is generally believed to spread at a faster rate than the northern ridge.

Seamount Chains and Aseismic Ridges

The aseismic Walvis ridge is manifest in Figure 3 as a band of moderate geoid roughness (30-50 cm). Directly to the south, the roughness rises to 50-60 cm over the Discovery Tablemount, a feature quite unrelated to the Walvis ridge. Although different models of isostasy have been proposed for Walvis ridge (Detrick and Watts [1979], Angevine and Turcotte [1980]), there is general agreement that the depth of compensation is shallow (15-30 km) for the Airy model. Figure 7 shows a sea surface height profile for a pair of two-minute pass segments crossing the Walvis ridge and Discovery tablemount. Also displayed is a bathymetric profile adopted from Figure 4 of Detrick and Watts [1979]. A moderate value of geoid roughness (28 cm) is obtained for the Walvis ridge segment, compared to 82 cm for the Discovery tablemount segment, even though the bathymetric relief (3 to 4 km) is comparable. The shallow compensation depth is apparently responsible for the modest value of geoid roughness over Walvis ridge.

In contrast, seamounts are not compensated at such shallow depths. Watts [1978] indicates simplified Airy compensation depths between 30 and 90 km for the Hawaiian-Emperor seamount chain, a feature which shows geoid roughness in excess of 100 cm.

Bermuda also appears as a significant high in the geoid roughness map (>80 cm), which tends to confirm the finding of Haxby and Turcotte [1978] of deep compensation for Bermuda. A striking high in the geoid roughness map (>110 cm) over the Tuamotu archipelago suggests that compensation is not shallow in this region either.

Error of Omission for Satellite Gravity Missions

The geoid roughness map can also be interpreted in terms of the error of omission of a satellite gravity (GRAVSAT) mission. The GRAVSAT mission objective is a detailed and accurate map of the earth's gravity field. This map is to have a resolution of 1 degree (220 km), and a precision corresponding to 10 cm RMS in geoid height. The planned configuration is for two satellites, seperated by about 330 km, in the same circular polar orbit at 160 km altitude. By precise measurement of the change in relative velocity between the satellites as they respond to anomalous gravity, one can calculate a global map of area mean gravity parameters. While the satellites' response to gravity anomalies is theoretically limited only by the system integration time and sensitivity, the parameterization of these measurements as area means of a certain size limits the mission accuracy. One limit is the omission error, which is the cumulative effect of those gravity anomalies of half-wavelength shorter than the size of the area mean gravity parameters; another limit is the error due to aliasing of the shorter wavelength orbital measurements

into the longer wavelength parameters. Our geoid roughness map gives a measure of the error of omission for a GRAVSAT mission parameterized for quasi-point quantities, insofar as our roughness values (wavelengths shorter than 2 arc degrees in 800 km arc segments) represent the geoid variance about a 1° area mean value determined by averaging of a dense set of uniformly distributed GRAVSAT measurements.

To quantify the expected reduction in our roughness values which might accrue from the use of true 1 area averages, consider the error of omission predicted for point measurements from Kaula's rule of thumb. This rule, integrated for all spherical harmonics of wavelength shorter than 220 km, yields an error of omission of 36 cm RMS (see Chovitz, 1973), for these wavelengths. If we assume the geopotential spectra behave as predicted by Kaula's rule of thumb for these short wavelengths, then we can apply Pellinen's averaging operator to these point value statistics to obtain their equivalent in area means For example:

$$\overline{\langle N^2 \rangle} = R_e^2 \sum_{\ell=2}^{\infty} \beta_\ell^{\,2} \, (2\ell+1) \, \sigma_\ell^2 \qquad (10)$$

$$\text{where } \beta_\ell = \left\{\frac{1}{1-\cos\Psi_o}\right\} \left\{\frac{1}{2\ell+1}\right\} \left\{P_{\ell-1}(\cos\Psi_o) - P_{\ell+1}(\cos\Psi_o)\right\} \qquad (11)$$

(see Tscherning and Rapp, 1974) for $\Psi_o = 0.564$ degrees (the spherical distance radius of an area equivalent to 1 degree by 1 degree), and where the P are the Legendre polynomials and σ_ℓ^2 is

the mean square fully-normalized geopotential coefficient of degree ℓ and Re is the radius of the earth.

Evaluation of equation 10, using Kaula's rule for σ_ℓ^2 and summing between degrees 180 and 1000, yields an error of omission in area mean geoid heights of 17 cm RMS instead of the 36 cm RMS predicted for point measurements. A similar reduction should accrue for the geoid roughness values computed and mapped in this study. On the other hand, our global average roughness value of 32 cm RMS is in excellent agreement with the degree variance of 31 cm RMS obtained by Wagner and Colombo [1979] from gravimetry and GEOS-3 altimetry for wavelengths shorter than 220 km.

Nevertheless, it appears that the error of omission for GRAVSAT may be less than 10 cm RMS for large areas of the oceans. The southeast Pacific ocean geoid is potentially the most accurately mapped by GRAVSAT, and the areas near trenches, and aseismic ridges less so.

CONCLUSIONS

The spectral analysis of Seasat altimeter data over short arc segments has been shown to yield geophysically interesting results. To a degree, the geoid roughness map generated from these analyses can be used, together with a bathymetry chart, to locate areas of shallow isostatic compensation.

The geoid roughness map can also be interpreted in terms of the error of omission in a satellite gravity (GRAVSAT) mission. In certain rather large areas of the southeast Pacific, the error of omission should be smaller than that over trenches and aseismic ridges. Insofar as the absolute roughness values can be trusted, we feel that the 10 cm geoid accuracy goal of the GRAVSAT mission can be satisfied best in the southeast Pacific.

ACKNOWLEDGEMENT

We would like to thank C. A. Wagner of the NOAA Geodetic Research Laboratory for his helpful edit and review of this manuscript.

REFERENCES

Abramowitz, M., and I. Stegun, Handbook of Mathematical Functions, Dover Publications, New York, 1970.

Angevine, C. L., and D. L. Turcotte, On the compensation mechanism of the Walvis ridge, Geophys. Res. Lett., 7, pp. 477-479, 1980.

Blackman, R. D., and J. W. Tukey, The Measurement of Power Spectra, Dover Publications, New York, 1958.

Brown, R. D., W. D. Kahn, and W. E. Himwich, Variability of geoid and ocean surface spectra From Seasat-1 altimeter data EOS, 62(8), Feb. 24, 1981, p 80.

Brown, R. D., Ocean tides at Cobb seamount from Seasat altimetry, J. Geophys. Res., ( ), this issue, 1982.

Chapman, M. E., Techniques for interpretation of geoid anomalies, J. Geophys. Res., 84, pp. 3793-3801, 1979.

Chapman, M. E., and M. Talwani, Comparison of gravimetric geoid with Geos-3 altimetric geoid, J. Geophys. Res., 84, pp. 3803-3816, 1979.

Chovitz, B.H., Downward continuation of the potential from satellite altitudes, Boll. di Geod. e Sci. Aff., XXXII(2), pp. 81-88, 1973.

Cochran, J.R., An analysis of isostasy in the world's oceans, 2: Midocean ridge crests, J. Geophys. Res., 84, pp. 4713-4729, 1979.

Detrick, R.S., and A.B. Watts, An analysis of isostasy in the world's oceans, 3: Aseismic ridges, J. Geophys. Res., 84, pp. 3637-3652, 1979.

Haxby, W.F., and D.L. Turcotte, On isostatic geoid anomalies, J. Geophys. Res., 83, pp. 5473-5478, 1978.

Kaula, W.M., Theory of Satellite Geodesy, Blaisdell, Waltham Mass., p98, 1966.

Leitao, C.D., and J.T. McGoogan, SKYLAB radar altimeter-short wavelength perturbations detected in ocean surface profiles, Science, 27 Dec., 1974, vol. 186, pp. 1208-1209, 1974.

Lerch, F.J., C.A. Wagner, S.M. Klosko, R.P. Belott, R.E. Laubscher, and W.A. Taylor, Gravity model improvement using GEOS-3 altimetry (GEM-10A and GEM-10B), paper presented at the 1978 Spring AGU Meeting, Miami, Florida, EOS, Trans. Am. Geophys. Union, 59(4), p260, 1978.

McKenzie, D. P., and C. Bowin, The relationship between bathymetry and gravity in the Atlantic Ocean, J. Geophys. Res., 81, pp. 1903-1915, 1976.

Tscherning, C. C. and R. H. Rapp, Closed power expressions for gravity anomalies, geoid undulations, and deflections of the vertical implied by anomaly degree variance models, Reports of the Department of Geodetic Science, Report No. 208, Ohio State Univ., July 1974.

Vening-Meinesz, F. A., The Earth's Crust and Mantle, Elsevier, p124, Amsterdam, 1964.

Wagner, C. A., The geoid spectrum from altimetry, J. Geophys. Res., 84, pp. 3864-3865, 1979.

Wagner, C. A., and O. L. Colombo, Gravitational spectra from direct measurements, J. Geophys. Res., 84(B9), pp. 4699-4712, 1979.

Watts, A. B., An analysis of isostasy in the world's oceans, 1: Hawaiian-Emperor seamount chain, J. Geophys. Res., 83, pp. 5989-6004, 1978.

FIGURES

Figure 1: Distribution of Seasat altimeter data tracks for 15 days from September 15 to 30, 1978.

Figure 2: Typical altimetric sea height power spectra showing the power-law fit compared to Kaula's rule.

Figure 3: Geoid Roughness Map: Global distribution of the square root of geoid peak power for wavelengths shorter than 220 km.

Figure 4: Altimetric sea height profiles over areas of high and low geoid roughness.

Figure 5. Comparison of spectra from areas of high and low geoid roughness showing the difference in slope.

Figure 6. Depth of compensation versus geoid roughness from a white-noise model of bathymetry assuming simplified Airy compensation.

Figure 7: Sea height profile and bathymetry for Discovery Tablemount and Walvis ridge. Note the difference in geoid undulation amplitude for comparable bathymetric relief.

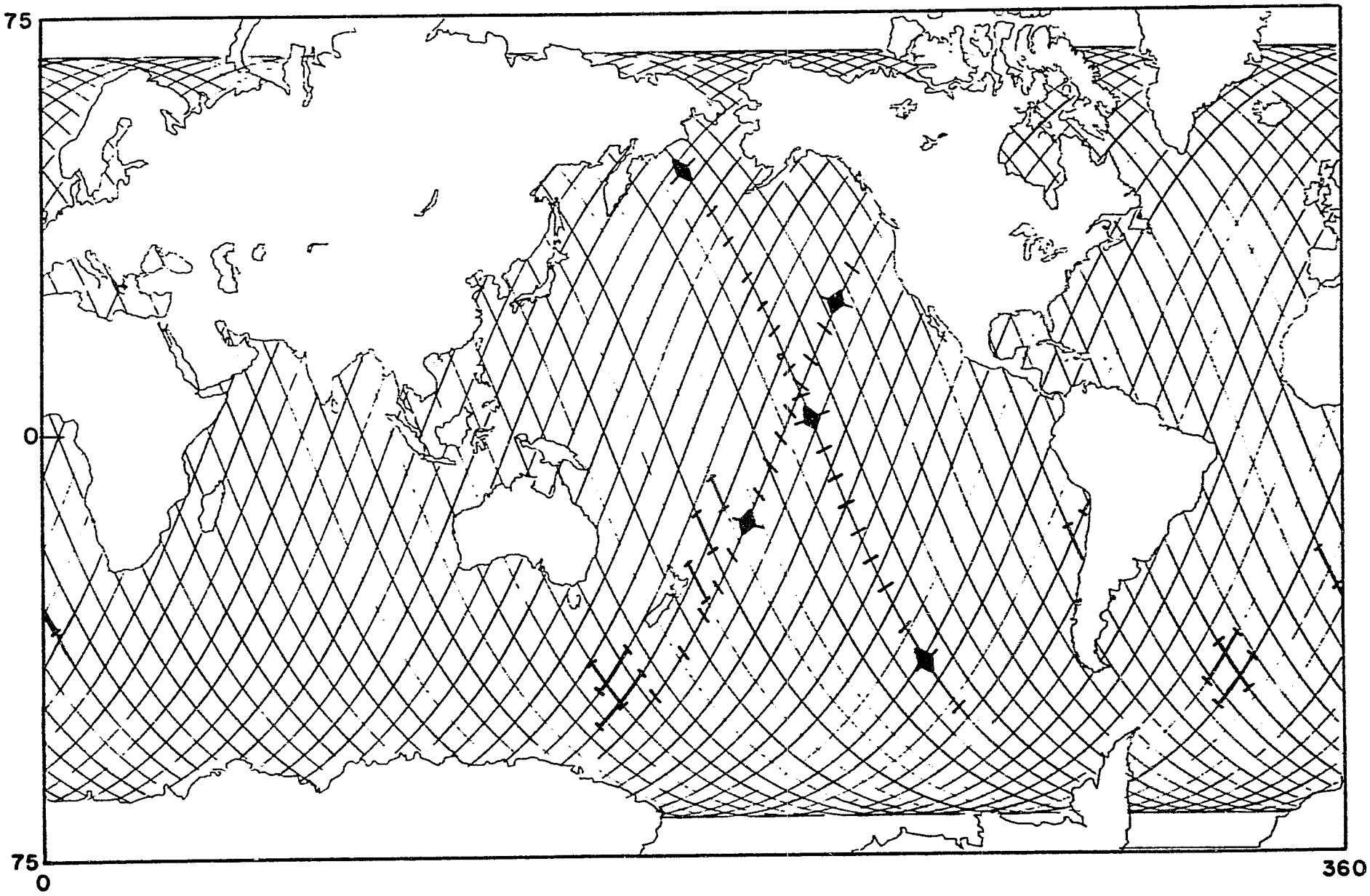

Figure 1.

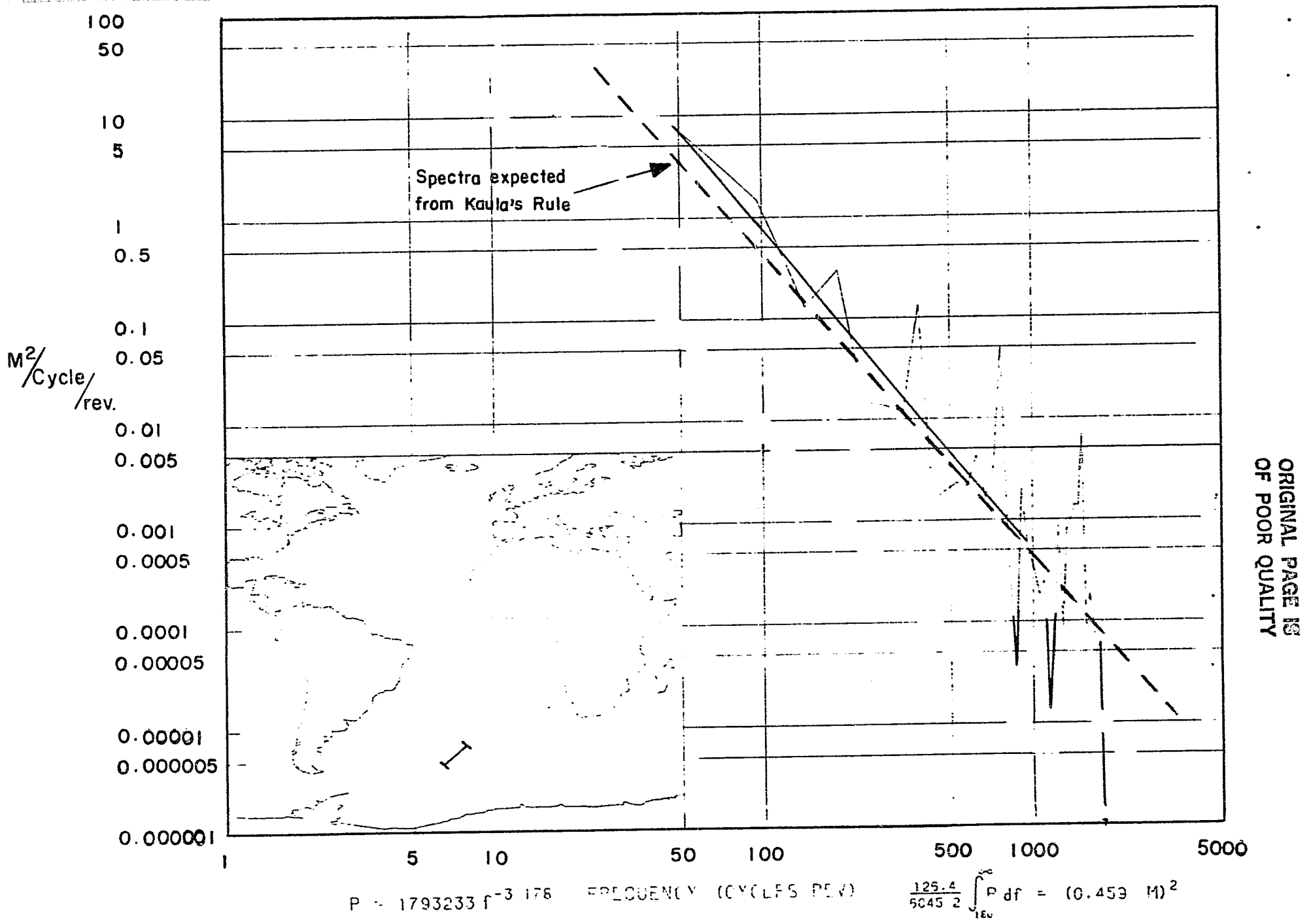
100
50
10
5
1
0.5
0.1
0.05
0.01
0.005
0.001
0.0005
0.0001
0.00005
0.00001
0.000005
0.000001
M²/Cycle/rev.
Spectra expected
from Kaula's Rule
1
5
10
50
100
500
1000
5000
P = 1793233 f^-3 178
FREQUENCY (CYCLES PER)
125.4/5045.2 ∫ P df = (0.459 M)²
ORIGINAL PAGE IS
OF POOR QUALITY

Figure 2

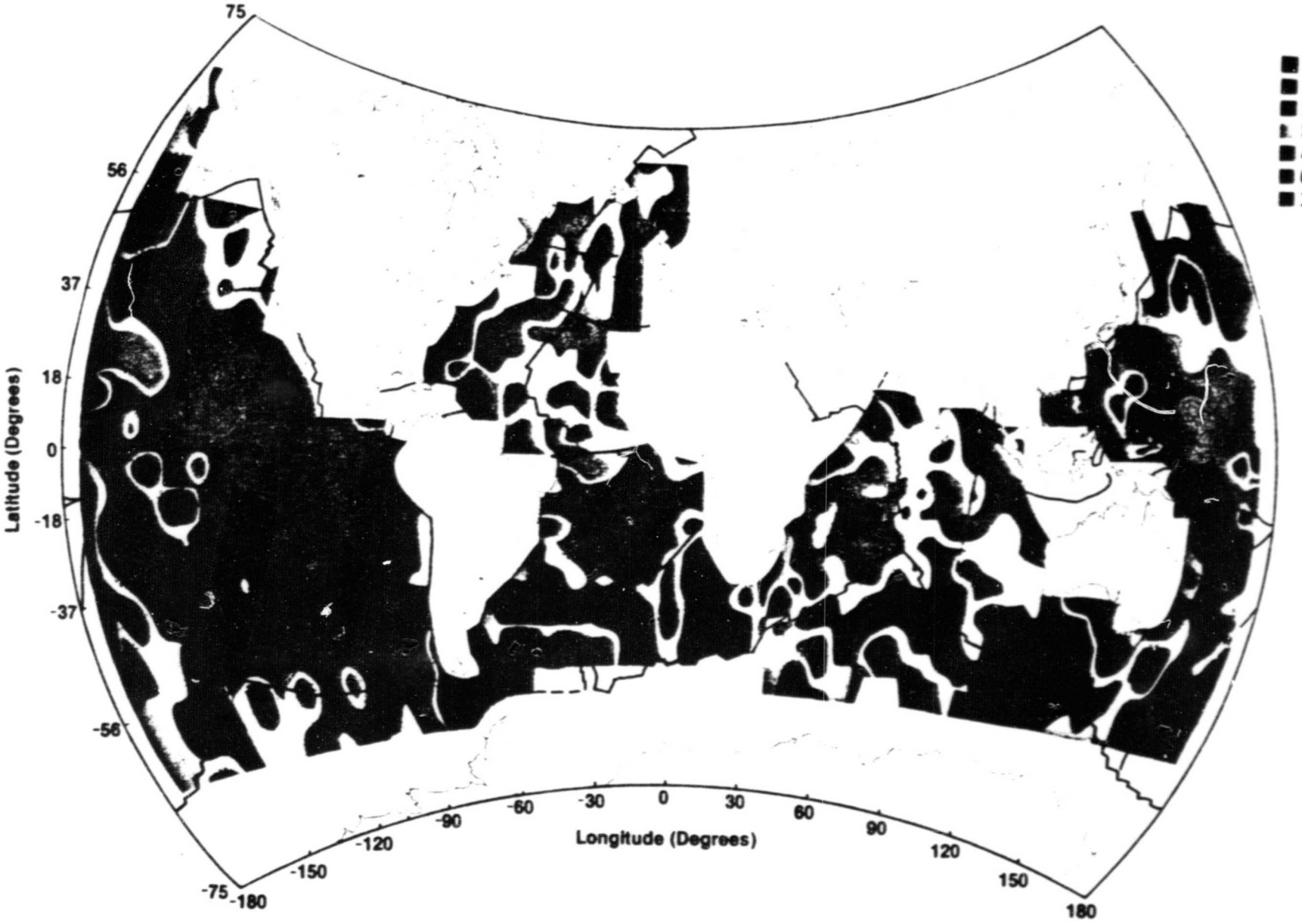

Figure 3.

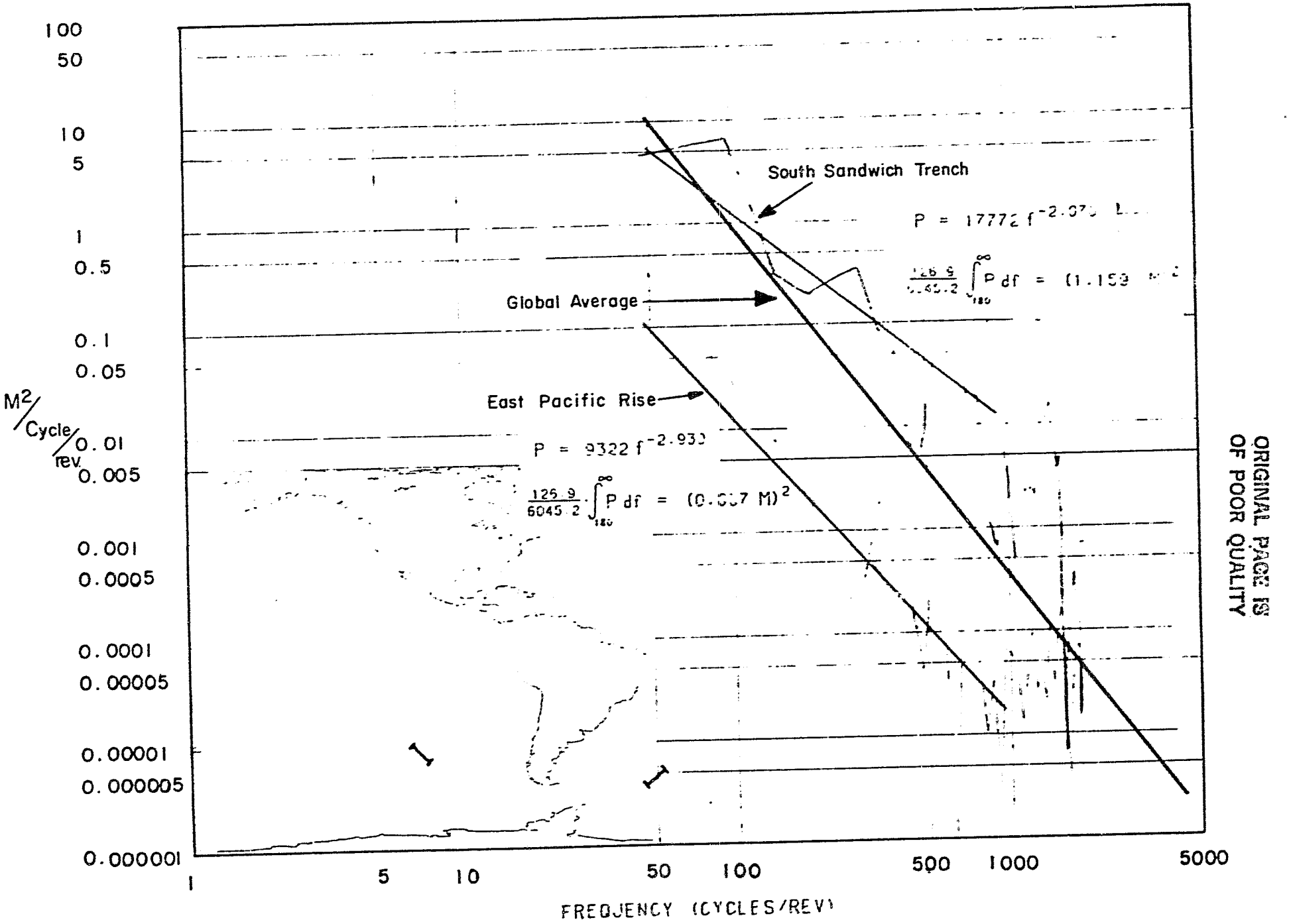
100
50
10
5
1
0.5
0.1
0.05
0.01
0.005
0.001
0.0005
0.0001
0.00005
0.00001
0.000005
0.000001
M²/Cycle/rev
South Sandwich Trench
P = 17772 f^-2.07
Global Average
East Pacific Rise
P = 9322 f^-2.93
1
5
10
50
100
500
1000
5000
FREQUENCY (CYCLES/REV)
ORIGINAL PAGE IS OF POOR QUALITY

Figure 4

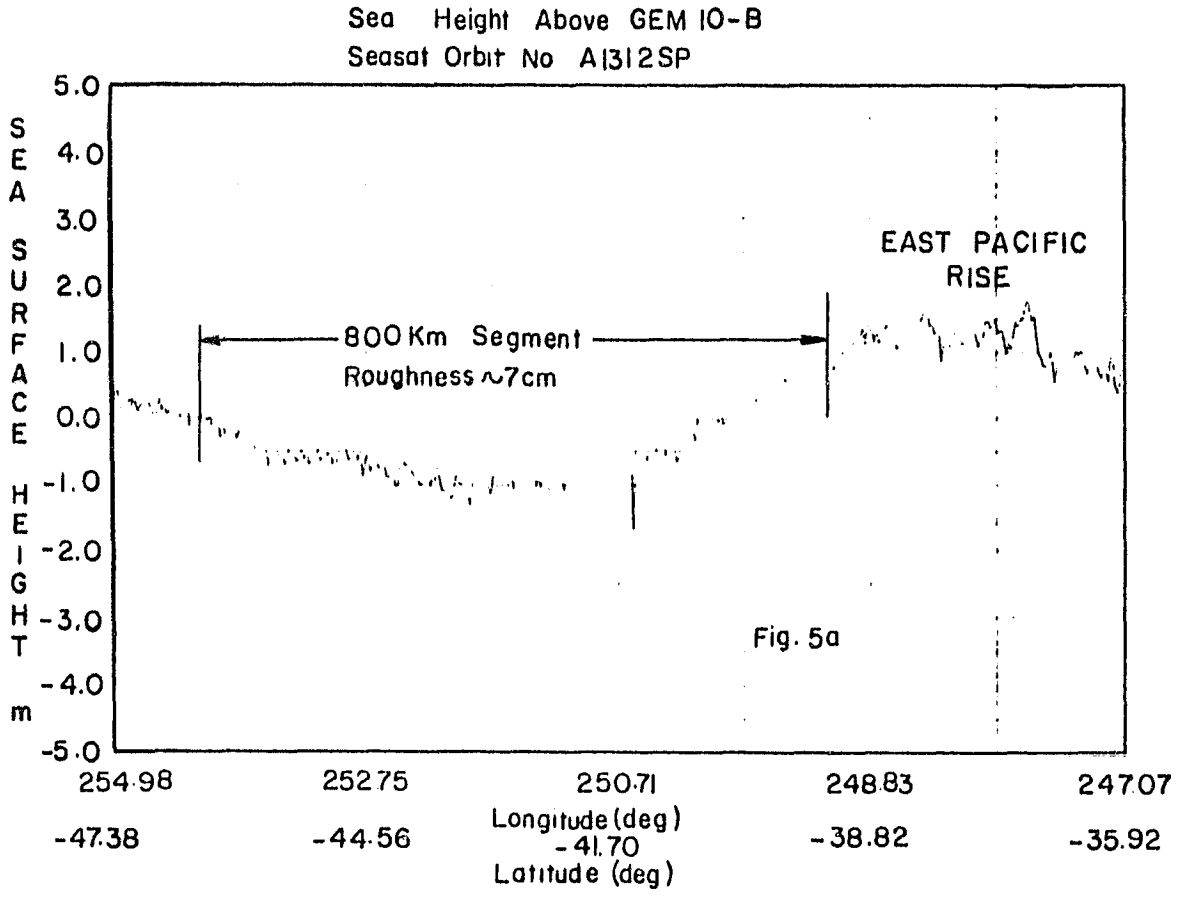

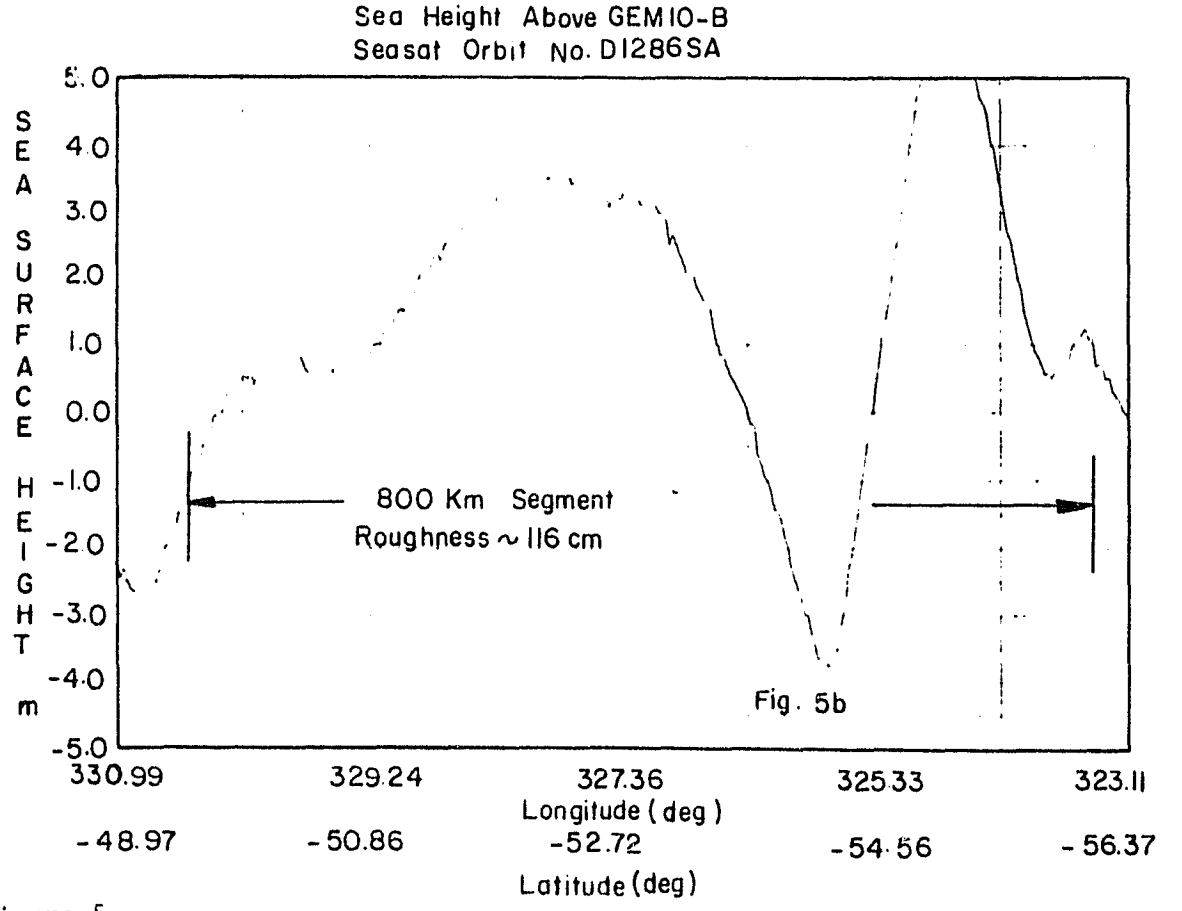

Figure 5

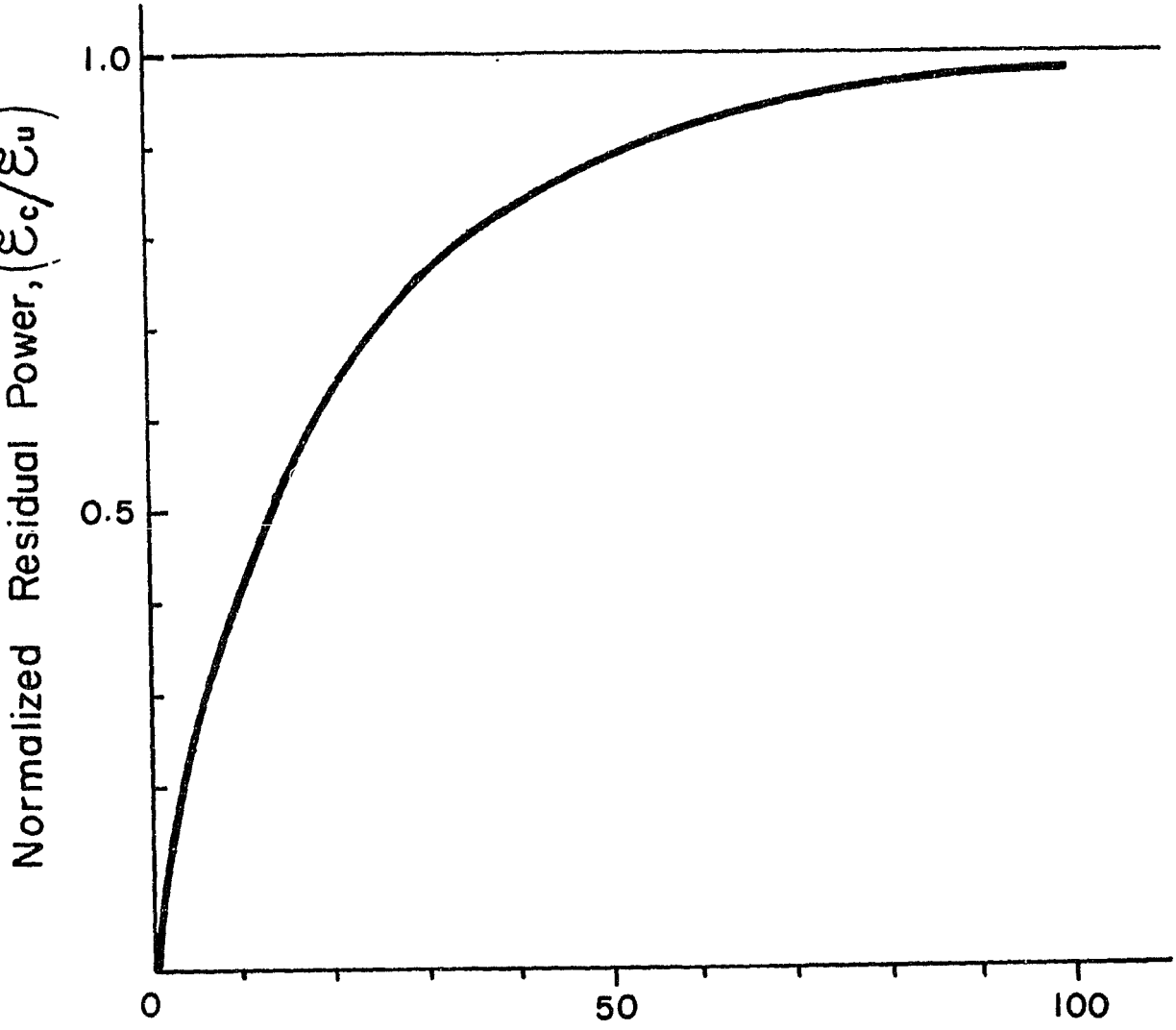

Simplified Airy Compensation

FIGURE. 6

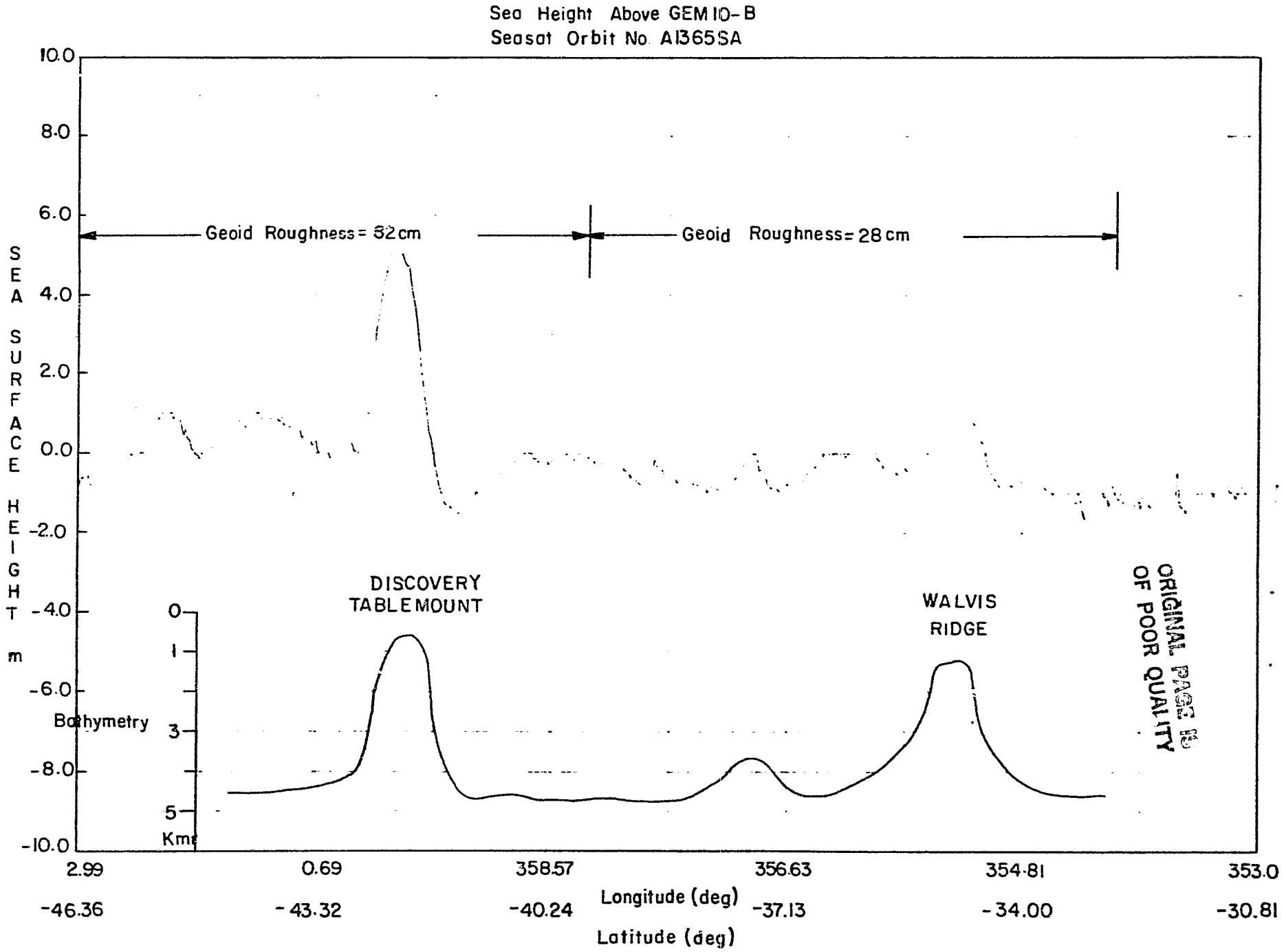
Sea Height Above GEM 10-B
Seasat Orbit No. A1365SA
10.0
8.0
6.0
4.0
2.0
0.0
-2.0
-4.0
-6.0
-8.0
-10.0
SEA SURFACE HEIGHT m
Geoid Roughness = 52 cm
Geoid Roughness = 28 cm
DISCOVERY TABLEMOUNT
WALVIS RIDGE
Bathymetry
0
1
3
5
Kms
ORIGINAL PAGE IS OF POOR QUALITY
2.99
0.69
358.57
356.63
354.81
353.0
-46.36
-43.32
-40.24
-37.13
-34.00
-30.81
Longitude (deg)
Latitude (deg)

Figure 7